# Roughening and melting of stepped aluminum surfaces

P. A. Gravil* and S. Holloway†
*Surface Science Research Centre, University of Liverpool, Liverpool, United Kingdom*
(Received 24 February 1995; revised manuscript received 3 November 1995)

The energetics and dynamics of the vicinal (113), (115), and (117) surfaces of aluminum have been investigated using a realistic many-body potential, based upon the effective medium theory, to describe the atomic interactions. These surfaces are found to show two distinct forms of thermal disordering. Firstly, above 700 K the surfaces undergo a roughening transition, characterized by a disordering of the step edge structure, the roughening temperature decreasing with decreasing step density. Secondly, above 900 K the surfaces undergo a melting transition, characterized by a complete disordering of the surface, the melting temperature increasing with decreasing step density. From studies of the step meandering, the time dependence of fluctuations in the step position were found to show a power-law dependence, $t^n$, where $0.25<n\leqslant 0.5$. This is consistent with two-dimensional diffusion on the surfaces, as observed experimentally. For noninteracting steps this corresponds to a time exponent of $n=0.5$. The reduced time dependence is then due to the repulsion between the steps.

## I. INTRODUCTION

No real surface is perfectly flat over macroscopic length scales. Misorientation of a crystal surface with respect to the major symmetry directions results in a structure of low-index terraces separated by atomic steps. Many of the unusual properties of stepped surfaces, such as their catalytic behavior, can be attributed to the low coordination of the step edge atoms. That the step edge atoms can be dislodged more easily than other surface atoms implies that as the temperature of a crystal is raised, the series of ordered steps will become full of defect kinks which will wander across the surface. This is the origin of the so-called roughening transition, a continuous phase transition of the Kosterlitz-Thouless (KT) type.[1] The KT transition is an infinite order phase transition; all temperature derivatives of the free energy are continuous. The roughening transition is associated with the proliferation of kinks, the transition temperature $T_R$ for roughening being that at which the free energy of step formation tends to zero. Above the transition temperature, kinks can spontaneously form and the step edges meander, the surface becoming delocalized, characterized by a logarithmic divergence of the step height-height correlation function.[2] Because thermal excitation at the step edges is much less costly than that from a terrace, the physical roughening occurs initially at the steps, while the terraces remain ordered until much higher temperatures. As a result, flat surfaces do not show signs of roughening until close to their melting point $T_M$. However, for vicinal surfaces, with periodic arrangements of steps, roughening can occur at temperatures well below the onset of surface melting, the two effects being distinct forms of thermal disorder.

Surface roughening on metal surfaces was first postulated from helium diffraction intensities for Cu (113), (115), and (117).[3–5] Direct evidence for such a transition then followed from helium atom scattering[6–12] and surface x-ray[13,14] studies for the $(11\{2m+1\})$ surfaces of both Ni and Cu. These surfaces showed changes in the diffraction line shapes consistent with a logarithmic divergence in the step height-height correlation function. The existence of a roughening transition has since been observed for many surfaces at temperatures ranging from $0.2T_M$ to $0.8T_M$, depending on the exact nature of the surface in question.

In recent years there has been a resurgence of interest in the energetics and dynamics of stepped surfaces, due mainly to the ability of the scanning tunneling microscope (STM), and other microscopies, to produce real-space images of such surfaces.[15–21] This has allowed measurements of real-time fluctuations in the step positions under equilibrium conditions. From such observations it is possible, theoretically, to determine the atomic mechanisms for step motion.[17,18] Several physical mechanisms for step motion have recently been described in terms of different rate limiting processes such as kink-diffusion or step-terrace exchange.[22,23] These different processes affect the time dependence and length scale of the step fluctuations, leading to a method of distinguishing the different processes experimentally. Such an analysis of the ''frizzy'' step edges observed on Ag(111) at room temperature using STM revealed that step motion occurs via kink diffusion along the step edge only.[18]

The equilibrium morphology of a surface is determined by the minimization of the surface tension (which at 0 K is the surface energy), while maintaining the surface orientation.[24] The variation of the reduced surface tension $f(\theta,T)$ with step density, $\tan\theta$ is given by[25]

$$f(\theta,T)=\gamma_0(T)+\frac{\beta(T)}{h}\,|\tan\theta|+g(T)|\tan\theta|^3,$$

where $\gamma_0(T)$ is the surface tension of the terraces between the steps, $\beta(T)$ is the free energy cost per unit length of step height $h$, and $g(T)|\tan\theta|^3$ is the free energy cost per unit area due to step-step interactions. To stabilize a stepped surface the reduced surface tension must decay with increasing step separation in such a way that, e.g., the (115) surface has a lower free energy than the corresponding linear combination of, e.g., (113) and (117) surfaces.

 

The interactions between the steps come from three sources. The first is stress mediated interactions caused by relaxations about the steps. The closer the steps are together, the fewer atoms there are between them to accommodate the relaxations, giving rise to long-range repulsive interactions between the steps.[26,27] Second, dipolar interactions, due to electrostatic dipoles induced along the step edges.[28] These interactions have recently been calculated, using density functional theory, for steps on (111) surfaces of aluminum, and were found to be weakly repulsive.[29] Finally, at high temperatures, there is an entropic contribution[30] arising from the fact that meandering steps cannot cross one another, since to do so would create an overhang that is energetically unfavorable. Bringing steps nearer to one another decreases the amount of wandering, and thus the configurational entropy, leading to an entropic repulsion between steps.

The equilibrium properties of a stepped surface, such as the terrace width and kink concentration, are then determined by a balance between the entropy gained by step meandering and the true energetic repulsion between the steps. Note that at any finite temperature a small concentration of kinks, and other defects, will always be thermodynamically stable because of the increased configurational entropy associated with their formation.

Many theoretical studies of stepped metal surfaces have concentrated on the energetics of step, kink, and defect formation.[5,31–35] Such calculations of surface energies are a necessary starting point for understanding the structure of stepped surfaces. However, because entropy is such an important factor in determining the thermodynamic properties of surfaces, energy calculations that correspond to zero temperature structures do not necessarily give a true understanding of the behavior of real surfaces. This issue is now being addressed directly by molecular dynamics (MD) simulations with realistic many-body potentials.[36,37] In this spirit we have performed MD simulations of the (113), (115), and (117) vicinal surfaces of aluminum with atomic interactions described by the effective medium theory (EMT).[38] The $(11\{2m+1\})$ vicinal surfaces, of which $m=1,2,3$ have the highest step densities, consist of (001) terraces, separated by (111) steps. On each terrace $m+1$ atomic rows are exposed. The simulations were performed at temperatures ranging from 0 K, to study the energetics, up to 1000 K, to investigate the dynamics of the roughening and melting transitions.

This paper is organized as follows. In Sec. II we briefly review the effective medium theory and outline the details of the simulations. The 0-K results for the surface energies, and relaxations, are presented in Sec. III. The general thermodynamic properties of the stepped surfaces are then discussed in Sec. IV, before we go on to consider the dynamics of step motion in greater depth in Sec. V. Finally, in Sec. VI we summarize the main findings of our study.

## II. MODEL AND METHOD

### A. The effective medium theory

The effective medium expression for the binding energy of a metal[38] is

$$E_B=\sum_i \left[E_C(\overline{n_i})+\Delta E_{\mathrm{AS}}(i)\right]+\Delta E_{1\text{-el}}, \qquad (1)$$

where the sum is over all atoms in the system. The first term, $E_C(\overline{n}_i)$, is the cohesive energy, the energy of the atom embedded in a homogeneous electron gas of density $\overline{n}_i$, defined as the average over a neutral sphere around atom $i$ of the electron densities from all the other atoms in the system. The final two terms are corrections for differences between the atom in the metal and in the reference system. The atomic-sphere correction energy, $\Delta E_{\mathrm{AS}}(i)$, describes the difference in the electrostatic interaction of the atom in the metal and in a close-packed fcc arrangement [where the electrostatic interactions are already included in the $E_C(\overline{n}_i)$ function]. The final term, the one-electron correction energy, $\Delta E_{1\text{-el}}$, is the difference between the covalent bond energy in the metal and in the reference system, and describes the discrete nature of the one-electron spectrum. In many cases, the first two terms alone are sufficient to provide a good description of the bulk and surface properties of simple metals, such as aluminum, for which the final term is generally assumed negligible.

In a previous paper on the self-diffusion of adatoms on the low-index surfaces of aluminum,[39] we showed the importance of covalent bonding during exchange mechanisms. The main finding was that covalent bonding was only important for systems with very low coordination, and was negligible in all other cases. For stepped surfaces, with narrow terraces, like those studied here, the repulsion between the steps prevents the diffusion of atoms away from the step edges into the low coordination sites on the terraces. Thus the situation addressed in the previous paper should never arise on the stepped surfaces studied here, and we may therefore assume covalent bonding, i.e., $\Delta E_{1\text{-el}}$, to be negligible. Further verification of this point will be given when we discuss the observed diffusion mechanisms on the stepped surfaces.

The effective medium theory has previously been used, with a great deal of success, to study the disordering and melting of the low-index surface of aluminum,[40–42] and other metals,[43] and we will briefly review the results: The observed surface stability follows the order in the packing density. The (110) surface disorders first via anharmonic effects (up to 750 K), then by adatom-vacancy formation, and finally by melting of the surface. The (100) surface also shows anharmonic effects, but no melting of the surface layers below the bulk melting point. Finally, the (111) surface is very stable up to the bulk melting point and even shows weak superheating effects. The bulk melting point of aluminum in these simulations, $T_M \approx 1050 \pm 50$ K, is higher than the experimental melting point (933 K). This is because the effective medium potential is optimized to the perfect fcc structure, and as a result, its description of the liquid is not as accurate as its description of the solid.

### B. Simulations

The computational cells employed in our MD simulations are of a slab geometry, with periodic boundary conditions in the $x$-$y$ plane, and the surface normal parallel to the $z$ direction. All simulations begin with the atoms in their perfect lattice positions, with the appropriate lattice constant $a(T)$ taken from previous constant pressure ($P=0$) simulations of the bulk. The dimensions of the computational cells are defined by $N_x \times N_y \times N_z$, Table I, where $N_x$ is the number of steps, $N_y$ is the number of atoms along the step direction, and $N_z$ is the number of dynamic "full layers;" on a $(11\{2m+1\})$

TABLE I. Dimensions of the (11{2m+1}) surfaces and of the computational cells used in the simulations. The $x$ direction and $y$ direction are taken as perpendicular and parallel to the step edges. The $z$ direction is normal to the surface plane, $\theta$ is then the angle between the surface normal and the (001) terrace normal. The computational cell for the (11{2m+1}) surface consists of $N_x$ steps, $N_y$ atoms long, and $N_z(m+1)$ crystal layers.

| Surface | $\theta$° | $x_0$ (Å) | $z_0$ (Å) | $N_xN_yN_z$ |
|---|---|---|---|---|
| (113) | 25.239 | 4.712 | 1.212 | 8×13×10 |
| (115) | 15.793 | 7.382 | 0.773 | 6×13×10 |
| (117) | 11.422 | 10.145 | 0.563 | 4×13×10 |
| (100) | | | 1.421 | 13×13×10 |

surface each full layer consists of $m+1$ ''partial layers'' (atomic rows). The layers are numbered from the topmost free surface; layer 1 is the first partial layer of atoms forming the step edges on an ordered surface.

The 0-K simulations were performed on a slab having two free surfaces. For the finite temperature simulations $N_{\text{static}}$ full layers on the bottom surface of the slab are kept at their perfect lattice positions to prevent spontaneous rotation of the system to expose a more stable surface. The static substrate acts as a perfect thermal insulator, and its thickness is greater than the range of the atomic interactions. The thickness of the dynamic slab, $N_z$, was adjusted to minimize interactions between either the two free surfaces or the surface and the static substrate, and it is assumed that bulk behavior is obtained away from the free surface(s). However, the static substrate has an artificially high order that will affect the adjacent dynamic layers, especially at very high temperatures, close to the melting point, when the number of disordered layers becomes comparable to the number of dynamic layers.

Since the overall size of the simulations (3000–4000 atoms) is restricted by computer considerations, and part of the study involved the investigation of the melting transition of the stepped surfaces, the area of the surface was limited by the requirement of an accurate description of subsurface layers, there being no direct interactions between the disordered layers and the static substrate layers. In most cases it was found that surfaces with areas of approximately 40×40 Å$^2$ [equivalent to 8, 6, and 4 steps on the (113), (115), and (117) surfaces, respectively, with 13 atoms along the step direction] were large enough to give a clear picture of the important physical processes. However, as with all molecular dynamics simulations, there are inherent limitations that should be highlighted. Firstly, the use of periodic boundary conditions places severe constraints on the extent of step meandering. Secondly, the step meandering process is slow relative to the time scale associated with molecular dynamics. Both these points will be discussed at the appropriate juncture.

The simulations were performed using molecular dynamics, the classical equations of motion for the atoms integrated using the velocity-Verlet algorithm,[44] with a time step of $1.0\times10^{-14}$ s to ensure numerical stability (i.e., energy conservation). The 0-K properties were calculated using the same molecular dynamics routine, modified to allow quasi-dynamic minimization; the kinetic energy of an atom is set to zero when the scalar product of its velocity and acceleration (i.e., force) is negative, corresponding to the atom moving out of a local minimum. This procedure quickly removes all excess energy from the system as the atoms relax to the minimum energy configuration. The minimization is considered complete when a system can run for several hundred time steps without further removal of energy, and the temperature is less than $1.0\times10^{-6}$ K. The surface relaxations and energies are calculated for defect-free systems, with perfectly ordered steps. Defects of opposite ''sign'' (forward and backward movement of the step edges) can be introduced into the system by moving atoms from one surface of the slab to the other, keeping the total number of atoms constant. As there are no direct interactions between the two free surfaces it follows that there are also no interactions between the defects. By comparing the energy of the relaxed defect system with that of the relaxed defect-free system, the defect energy can be found exactly.

For the finite temperature studies, the systems were equilibrated to the simulation temperature $T_S$ by stochastic thermalization.[44] Equilibration takes several thousand time steps, with massive stochastic collisions being applied at regular intervals. This is the most efficient way of equilibrating a system of atoms, and reduces the risk of any collective motion of the atoms parallel to the surface. Following equilibration, the system is allowed to evolve microcanonically for a further several thousand time steps, with configurations saved every 10 time steps for subsequent analysis.

## III. ZERO TEMPERATURE CALCULATIONS

### A. Surface relaxations

The percentage interlayer relaxations, defined as

$$d_{i,i+1}=100\,\frac{(z_i-z_{i+1})-z_0}{z_0}, \tag{2}$$

where $z_0$ is the unrelaxed bulk interlayer spacing, are presented in Table II. That the magnitude of the relaxations appears to increase with terrace width is an artifact of the definition of $d_{i,i+1}$, due to the decrease in bulk interlayer spacing $z_0$ with increasing terrace width, Table I. The magnitudes of the physical displacements actually decrease with increasing terrace width.

TABLE II. Calculated percentage interlayer relaxations at 0 K for the first 3(m+1) crystal layers on the (11{2m+1}) surface.

| Surface | $d_{1,2}$ | $d_{2,3}$ | $d_{3,4}$ | $d_{4,5}$ | $d_{5,6}$ | $d_{6,7}$ | $d_{7,8}$ | $d_{8,9}$ | $d_{9,10}$ | $d_{10,11}$ | $d_{11,12}$ | $d_{12,13}$ |
|---|---|---|---|---|---|---|---|---|---|---|---|---|
| (113) | −6.8 | +4.0 | −2.9 | +2.1 | −1.1 | +0.9 | | | | | | |
| (115) | −8.0 | −5.2 | +8.4 | −3.2 | −3.2 | +4.5 | −1.4 | −1.3 | +2.0 | | | |
| (117) | −8.3 | −4.9 | −5.9 | +13.1 | −3.6 | −3.1 | −3.3 | +7.1 | −1.2 | −1.9 | −1.2 | +3.6 |

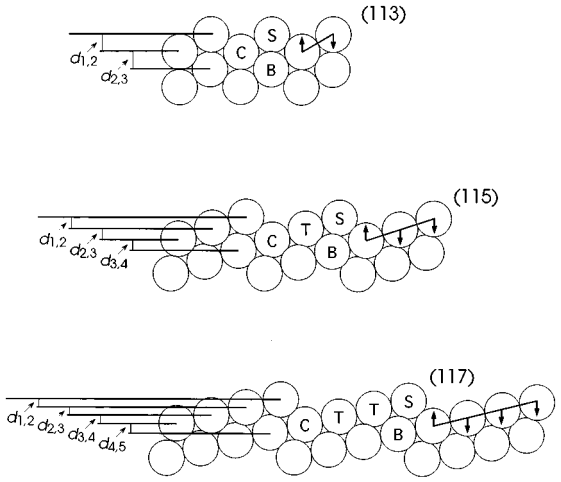


FIG. 1. Views of the $(11\{2m+1\})$, $m=1,2,3$, surfaces projected onto the $x$-$z$ plane, showing the nature of the interlayer relaxations. Notice that the interlayer spacing decreases with increasing terrace width. The step edge atoms ($S$), the terrace atoms ($T$), the corner atoms ($C$), and the subsurface or bulklike atoms ($B$), as labeled, refer to the ordered phase.

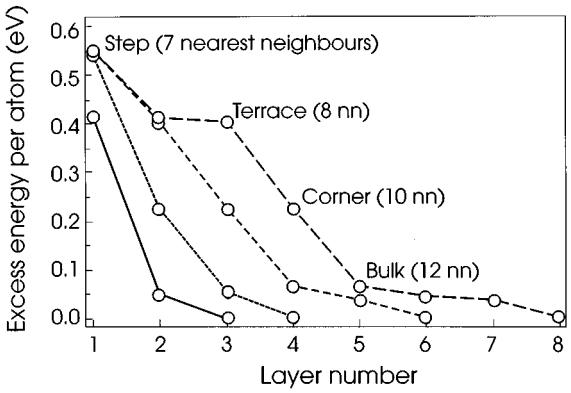


FIG. 2. The excess energy per atom as a function of position for the (100) (solid line), (113) (dotted line), (115) (short-dashed line), and the (117) (long-dashed line) surfaces. The surfaces are perfectly ordered at 0 K. The respective energies of the step edge atoms ($S$), the terrace atoms ($T$), the corner atoms ($C$), and the subsurface or bulklike atoms ($B$) are comparable on all three stepped surfaces. Also the energy of the terrace atoms is consistent with that of an atom in the (100) surface.

The surface layers show a repeated pattern of inward and outward relaxations, with a periodicity equal to the number of atomic rows per terrace, and an exponential damping in magnitude away from the surface. For a surface with terraces $m+1$ atomic rows wide, the top $m$ layers of atoms show inwards relaxations, the effect being greatest for the first layer; the atoms that constitute the step edges, being particularly exposed, are strongly attracted to their neighbors; while the final $m+1$ layer of atoms, the corner atoms, being partially covered by the step edge atoms of the next terrace, have large outward relaxations. Thus the layers of atoms on a stepped surface attempt to flatten out, as illustrated by the arrows in Fig. 1. Similar relaxations have been found both experimentally and theoretically for stepped surfaces of other metals.[31,33,36,45,46]

### B. Surface energies

The surface energy $\gamma_s$, defined as the excess energy per atom per unit surface area, is given by

$$\gamma_s=\frac{E-N\varepsilon_b}{2L_xL_y}, \tag{3}$$

where $E$ is the total energy of the system of $N$ atoms obtained from the energy minimization, $\varepsilon_b$ is the energy of a bulk atom, and $L_xL_y$ is the area of the surface. The factor of 2 accounts for the two free surfaces of the slab used in the calculation.

The calculated surface energies are summarized in Table III. At low temperatures the surface energy arises from the reduced coordination, and thus bonding, of the atoms at the surface relative to those in the bulk. As such, it is a measure of the stability of the surface; the higher the surface energy, the less stable the surface. Thus the (113) surface, having the highest density of sevenfold coordinated step edge atoms per unit area, is the least stable. As the terrace width increases, the surfaces become more stable, and in the limit of infinitely wide terraces, the surface energy will approach that of the flat (100) surface.

We can also calculate the excess energy per atom as a function of position, i.e., layer, on the stepped surfaces:

$$\gamma_l=\varepsilon_l-\varepsilon_b, \tag{4}$$

where $\varepsilon_l$ is the energy of an atom in layer $l$, and $\varepsilon_b$ is again the energy of a bulk atom. The results are shown in Fig. 2. Again the step edge atoms have the highest excess energies, 0.55 eV, due to their low coordination, seven nearest neighbors (7 NN). A terrace atom with 8 NN has an energy of 0.42 eV, and a corner atom with 10 NN an energy of 0.23 eV. The

TABLE III. Calculated surface energy $\gamma_s$, step-step repulsion $w_m$, kink formation energy $W_0$, and adatom-vacancy pair formation energy $E_{\text{defect}}$, at 0 K for the $(11\{2m+1\})$, $m=1,2,3$, surfaces.

| Surface | $\gamma_s$ (J m$^{-2}$) | $w_1$ (K) | $w_2$ (K) | $w_3$ (K) | $W_0$ (K) | $E_{\text{defect}}$ (eV) |
|---|---|---|---|---|---|---|
| (113) | 0.995 | 115.7 | | | 1155.1 | 0.423 |
| (115) | 0.988 | | 21.7 | | 1091.4 | 0.387 |
| (117) | 0.979 | | | 12.3 | 1140.0 | 0.352 |
| (100) | 0.608 | | | | | |

atoms in the subsurface layer with a full 12 NN, having only lost a few of their next-nearest neighbors, have excess energies of less than 0.06 eV.

### C. Kink formation energy and step-step interaction

To understand the dynamics of stepped surfaces, i.e., the step roughening and meandering processes, it is first necessary to develop an understanding of the energetics of kink formation. Villain *et al.*[5,31,47] were the first to associate the energy of a stepped surface with the number of kinks and the degree of step-step repulsion present. They developed a model for the energy of a stepped surface based on two parameters: the kink creation energy on a step edge $W_0$ and the repulsion energy per unit length between steps, i.e., the energy required to move a step-edge atom one atomic row closer to another step, $w_m$, where $m+1$ is the number of atomic rows originally separating the two steps.

The step-step interaction energy $w_m$ can be calculated directly in our simulations by moving one complete atomic row of step-edge atoms (i.e., $N_y$ atoms) from the upper surface of the slab to the lower surface. The energy difference between this system and the defect-free system then gives $w_m$. Similarly, the kink formation energy $W_0$ can be calculated by systematically moving step-edge atoms from the upper surface of the slab to the lower surface. If $n$ atoms ($n=1,\ldots,N_y/2$) are moved from one surface to the other, creating two pairs of kinks (one positive and one negative) both of length $n$, then the energy difference is equal to $4W_0+2nw_m$.

The calculated $w_m$ and $W_0$ are summarized in Table III. The step-step interactions $w_m$ are all positive, i.e., repulsive, decreasing with increasing terrace width. Thus the three surfaces are stable. The kink formation energies $W_0$ for the three surfaces are all of the same order of magnitude, independent of terrace width and kink length, and are considerably larger than the respective $w_m$. Note that $W_0$ and $w_m$ are calculated at 0 K, and the effect of thermal motion and disorder on the two parameters is unknown. Experimentally, it is very hard to obtain consistent values for the two parameters due to the continuous nature of the roughening transition.[5,8–10,12,13,48,49]

Finally, the formation energies of a single step edge adatom-vacancy pair for the three surfaces are also given in Table III, and can be seen to decrease with increasing terrace width due to decreasing step-step repulsion as discussed above.

As we have already mentioned, the long-range repulsion between steps is necessary to ensure the stability of the surfaces at low temperatures. The ability of the EMT to give what appear to be, in the absence of any experimental data, reasonable values for the step-step interactions, and other physical properties, is a good indication of its suitability for such studies.

## IV. FINITE TEMPERATURE SIMULATIONS

Before starting the analysis of the dynamics of the stepped surface we can first visualize the results of our simulations by means of snapshots of the atomic positions from the MD trajectories. Figure 3 shows some snapshots for the (115) surface at various temperatures. At 600 K the surfaces

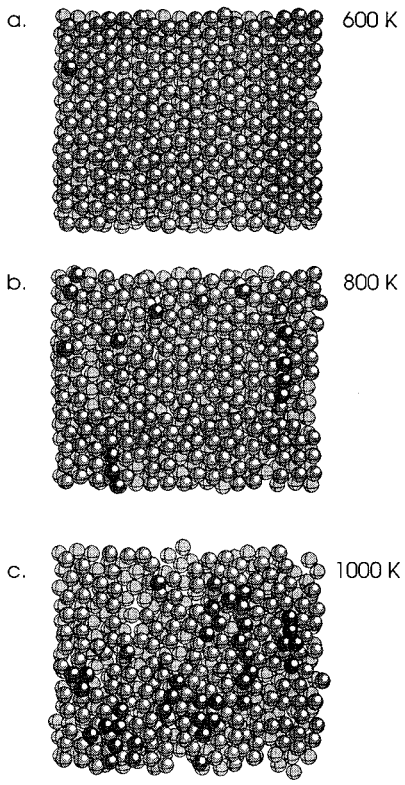


FIG. 3. Snapshots of the atomic configurations generated by the molecular dynamics simulations for the (115) surfaces. The darkest shading corresponds to adatoms, the lightest to subsurface atoms. Three different phases exist on the stepped surfaces: the ordered phase, below 600 K; the rough phase, around 800 K; the molten phase, around 1000 K.

are well ordered with straight steps; this is the ordered phase. As the temperature increases kinks start to appear in the step edges, 800 K. The first signs of disordering are clearly restricted to the step edges, the terraces remaining well ordered until much higher temperatures. As the temperature continues to increase the surfaces become more and more disordered as the extent of the step meandering increases. This is the rough phase. At 1000 K the surfaces appear completely disordered as the result of surface melting.

### A. Layer structure

To investigate the variation of the properties of the stepped surfaces with temperature we show first in Fig. 4 the average atomic densities projected onto the $z$ axis, normal to the surface, at various temperatures. The most striking feature of these results is the pronounced grouping of the first $m+1$ partial layers forming the $(11\{2m+1\})$ surface, and of subsequent layers. This is due to the relaxation effects already discussed. Above 600 K there is a gradual change in the density profiles near the surface, which now start to slowly spead into the vacuum at the interface. This is due to the presence of atoms in positions above the surface, associated with the formation of additional surface layers that are absent at lower temperatures. In simulations of low-index surfaces, atoms in layers above the surface are generally referred to as *adatoms*, with associated *vacancies* in the surface layers. In our discussion of the properties of the stepped

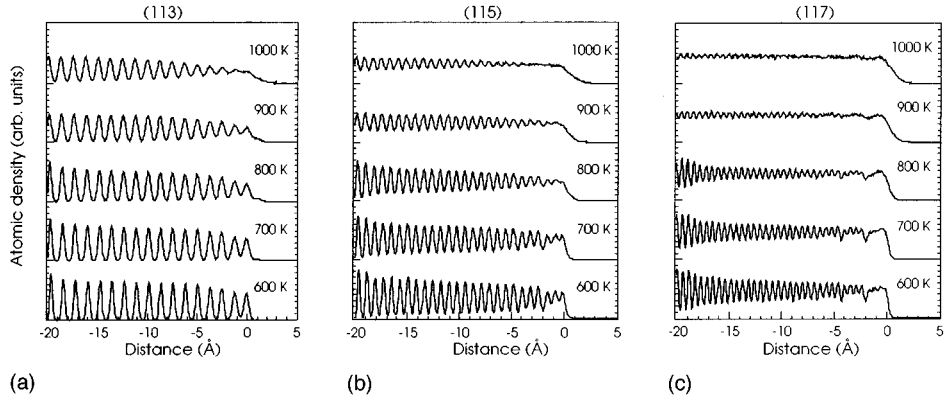


FIG. 4. Average atomic densities projected onto the $z$ axis normal to the surface for the (a) (113), (b) (115), and (c) (117) surfaces. Notice the grouping of the $m+1$ layers on the $(11\{2m+1\})$ surface. At 700 K, and above, the density profile of the surfaces changes with the presence of atoms in positions above the surface, located at $z=0$ Å for the perfectly terminated bulk, due to surface roughening. Surface melting can be implied from the loss of structure in the topmost surface layers around 1000 K, although this is complicated on the higher-index surfaces due to the large vibrational amplitudes of the atoms compared to the interlayer spacings.

surfaces we shall retain this convention, but emphasize that these adatoms are now formed by the motion of the step edges; motion of step-edge atoms one, or more, atomic rows forward from their position in the ordered phase is associated with the creation of step-edge adatoms, and equivalently, motion of step-edge atoms one, or more, atomic rows back with the creation of step-edge vacancies. The adlayers are therefore the result of surface roughening and are not directly attributable to the melting of the surface, as on low-index surfaces.[40] At very high temperatures, close to the bulk melting point, there is a disintegration of all layer structure near the surface. This loss of structure is attributed to the formation of a liquidlike interface on the surface, the thickness of which increases with temperature, and is associated with surface melting.[40–43,50,51] A cautionary word; although there is undoubtedly some melting of the surfaces at high temperatures, above ~900 K, the picture is complicated on the higher-index stepped surfaces by the large vibrational amplitudes of the surface atoms compared to the interlayer spacings.

At elevated temperatures, the surfaces are highly mobile, and at the end of a trajectory an atom may be found at a considerable distance, and in a different layer, from its original lattice position. As an error in the assignment of layer number for an atom can cause a substantial error in the calculated properties of a layer, it is necessary to reassign layer numbers for all atoms in order to correctly analyze the MD trajectories. Further, the assignment of lattice positions allows the time dependence of fluctuations in step-edge position to be determined, enabling us to study the dynamics of step meandering. Since, as we shall see, the system always retains some degree of crystalline order, even at the highest temperatures, it is possible to assign layer numbers and lattice positions by mapping the positions of all the atoms onto a perfect lattice, i.e., assigning layer and position according to the nearest lattice site.

### B. Defects in layers

The average layer occupations as a function of temperature, $\langle N_l \rangle_T$, are shown in Fig. 5(a). As the temperature increases above 600 K there is a gradual increase in the occupation of successive adlayers, and an associated decrease in

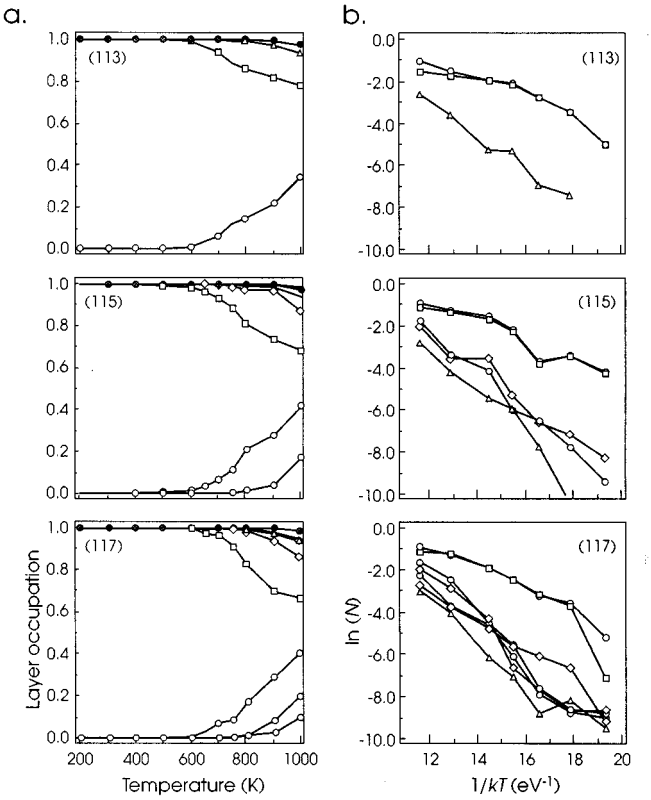


FIG. 5. (a) The average layer occupations as a function of temperature for the adlayers and first few crystal layers on the three surfaces. The symbols, which for the crystal layers refer to the position of the layer in the ordered phase, are open circles for adlayers, squares for the step edges (i.e., the first crystal layer), diamonds for the terraces, triangles for the corners, and solid circles for all other subsurface atoms. The increased occupation of adlayers and decreased occupation of crystal layers above 600 K is due to surface roughening as described in the text. (b) The natural logarithm of the adatom-vacancy concentration, $N$, for the adlayers-crystal layers, as a function of $1/kT$. The adatom-vacancy formation energies are estimated to be 0.44, 0.39, and 0.36 eV, for the (113), (115), and (117) surfaces, respectively.

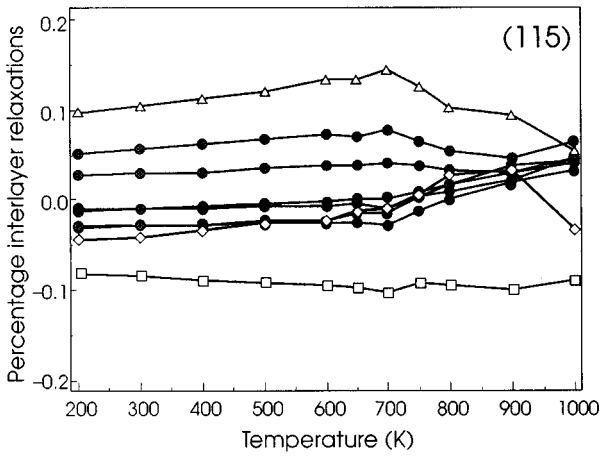


FIG. 6. Percentage interlayer relaxations as a function of temperature for the surface layers on the (115) surface. The symbols are defined in Fig. 5. The relaxations of adlayers, not shown, are negative, increasing in magnitude with increasing temperature. For all three surfaces, the general trend is for an outward expansion of the surface layers, corresponding to an increased thermal expansion coefficient of the surface.

the occupation of the surface layers, due to the formation of kinks and step meandering. The adatom-vacancy concentrations for each layer have been plotted in the Arrhenius form, Fig. 5(b). At low concentrations the data can be fitted to straight lines, consistent with a thermally activated process. The energy to create an adatom in the first adlayer (and associated vacancy) is equivalent to the energy to create a vacancy in the first surface layer (and associated adatom). The divergence at high concentrations results from the correlated nature of step fluctuations. The adrows and vacancy defects are no longer individual adatoms or vacancies but trains of such defects which have a lower energy per step edge adatom-vacancy pair than was calculated for single pairs, see Table III. The formation energies for an adatom (and associated vacancy) in the first adlayer are estimated to be 0.44, 0.39, and 0.36 eV for the (113), (115), and (117) surfaces, respectively, which are in surprisingly good agreement with the values calculated at 0 K, Table III.

In conclusion, there is a gradual increase in the occupation of adlayers, and a decrease in the occupation of surface layers, due to the formation of kinks and defects, at temperatures above 600 K on all three surfaces. Since the adatom-vacancy pair formation energies decrease with increasing terrace width, it follows that the surface roughening temperature also decreases with increasing terrace width. Unfortunately we cannot be more specific on this point due to the finite sizes of the systems studied.

### C. Relaxations and vibrational amplitudes

The calculated percentage interlayer relaxations as a function of temperature are shown in Fig. 6 for the (115) surface. Similar behavior is observed on the other two surfaces, where it is also found that relaxations are strongly temperature dependent. This directly reflects the anharmonicity of the surface layers. If the thermal expansion coefficient of the surface region was the same as that of the bulk, the relaxation curves would all be horizontal lines. This is clearly not the case. At low temperatures, the repeated pattern of inward and outward relaxations, as observed at 0 K, is visible. As the temperature increases, the general trend is an outward expansion of the layers forming the surface. The increased outward surface relaxations then correspond to an enhancement of the thermal expansion coefficient of the surface. The exception is for the topmost surface layer, which shows increased contraction as the atoms forming the step edge in the ordered phase try to maximize their coordination by forming a flat (step-free) surface. Note that such a surface would be highly distorted.

Above 700 K, the forward and backward motion of the step edge increases the coordination of some atoms in the first few layers while reducing that of other atoms in deeper layers. Under such conditions the nature of the interlayer spacings changes due to the large variety of different configurations experienced by the atoms in the topmost surface layers. The adlayer relaxations, not shown, are all negative, increasing in magnitude with temperature, consistent with the idea of the surface trying to flatten out. The interlayer relaxations of the partial layers forming the second, and deeper, full layers are much simpler, showing enhanced thermal expansion with increasing temperature.

The vibrational amplitudes of the atoms can be calculated directly from the distribution of the positions of the atoms in a layer:

$$\sigma^2_{\alpha,l}=\left\langle \frac{1}{N_l}\sum_{i=1}^{N_l}[\mathbf{R}_{\alpha,i}-\overline{\mathbf{R}}_{\alpha,i}]^2 \right\rangle, \tag{5}$$

where $\underline{\mathbf{R}}_{\alpha,i}$ $(\alpha=x,y,z)$ is the position of the atom at lattice site $i$, $\mathbf{R}_{\alpha,i}$ is the equilibrium position of the lattice site $i$, $N_l$ is the instantaneous number of atoms in layer $l$, and average $\langle\,\rangle$ is over the MD trajectory. Figure 7 shows the mean-square displacements (MSD) in the $x$, $y$, and $z$ directions as functions of temperature, for the three surfaces. Note that the $x$ and $z$ directions are defined by the unit cell of the stepped surface, and not by that of the flat terraces.

The vibrations are clearly anharmonic, scaling nonlinearly with temperature. The degree of anharmonicity increases with temperature being largest for the first $m+1$ layers, i.e., the exposed surface, and decreases rapidly for deeper layers. There are no discontinuities in the calculated amplitudes associated with either the roughening or melting transitions, although there are slight increases in the temperature dependence of the amplitudes in both the $x$ and $y$ directions, above 600 and 900 K, and in the $z$ direction also above 900 K, on all three surfaces, which are undoubtedly related to these phenomena.

The amplitudes in the $x$ and $y$ directions, perpendicular and parallel to the step edges in the plane of the surface, are comparable, being a few percent larger in the $x$ direction, for all layers on all surfaces. This is surprising, considering that the first partial layer of atoms, those which on the ordered surface constitute the step edge, are unbounded on the lower terrace side in the $x$ direction. There are two probable factors contributing to this observation: firstly, relaxation effects, the adatoms being strongly attracted to their neighbors acts to confine them, and secondly step-edge repulsion limits the motion of the step-edge atoms perpendicular to the steps

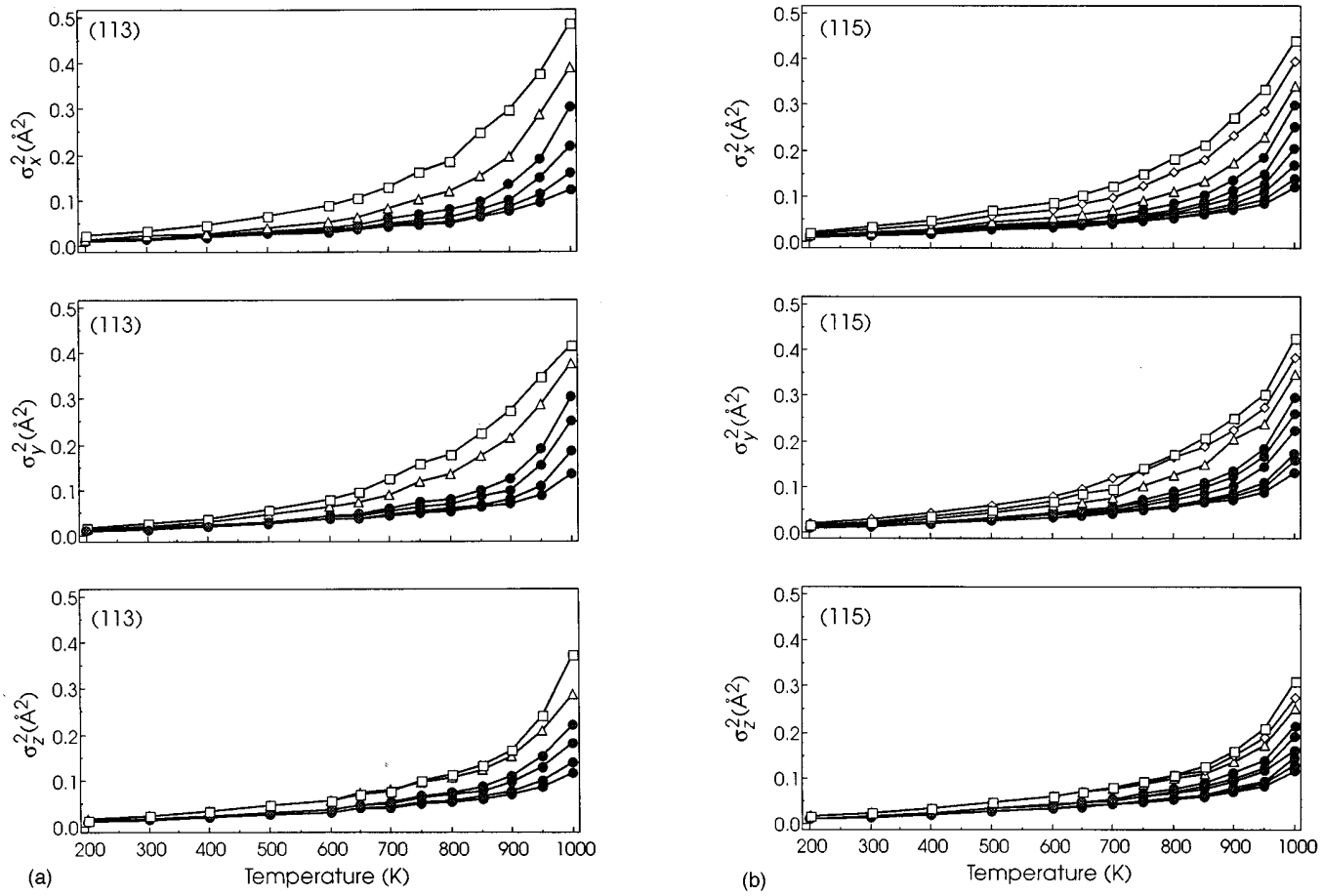


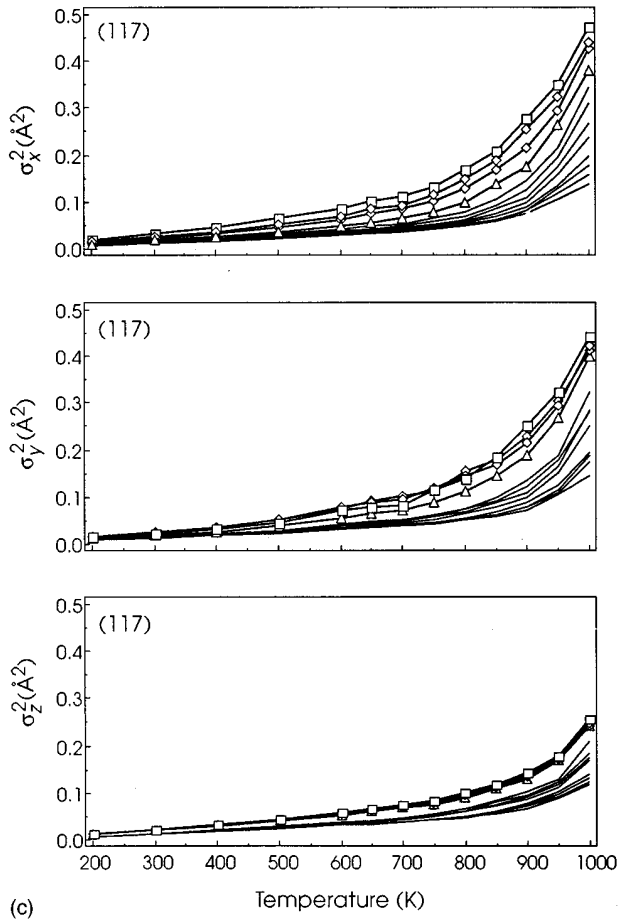


FIG. 7. The mean-square vibrational displacements in the $x$, $y$, and $z$ directions for the first $3(m+1)$ crystal layers on the (a) (113), (b) (115), and (c) (117) surfaces. The symbols are as defined in Fig. 5. The vibrations are anharmonic, the degree of anharmonicity increasing with temperature. The magnitude of the vibrations in the $x$ and $y$ directions are comparable on all three surfaces, whereas the magnitude of the vibrations in the $z$ direction decreases with increasing terrace width reflecting a change from interlayer to intralayer bonding.

(although this effect would be hard to quantify). In the $y$ direction there is grouping of the $m+1$ partial layers forming the full layers, that is, atoms in the surface layers have equivalent amplitudes parallel to the steps irrespective of their position relative to the step. In the $x$ direction the amplitudes decrease uniformly away from the surface, the atoms forming the step edges in the ordered phase having the largest amplitudes. For the (115) and (117) surfaces, the first partial layer, the step-edge atoms, shows reduced amplitudes in the $y$ direction compared to the terrace atoms, below 700 K. This is also attributed to the relaxation effects and the energetic step-step repulsion, which are then gradually swamped by the thermal energy of the surface atoms above 700 K.

The displacements in the $z$ direction, perpendicular to the surface, are considerably smaller than the in-plane displacements, with this effect becoming more pronounced with increasing terrace width. On the (117) surface the in-plane mean-square displacements are a factor of 2 greater than the out-of-plane amplitudes of the highest temperatures. They also show the same $m+1$ grouping of partial layers, going many layers deep into the surface. Thus as the terrace width increases, the atoms become more tightly bound with atoms in the same layer than with those in the adjacent layers. Indeed, the vibrational amplitudes for the atoms in a (117) surface are comparable with those in a (100) surface.[42]

There are two problems inherent in MD simulations of this kind, which must taken into account when interpreting MSD results. Firstly, the finite size of the computational cells and the periodic boundary conditions may generate collective motion of the atoms in the close-packed directions, e.g., along the atomic rows, which leads to an overestimate of the MSD in that direction. However, this effect is expected to be small for the large systems used in this work, and the chances of generating collective vibrational modes are greatly reduced by the use of stochastic thermalization. Secondly, since we have not extrapolated our results to the thermodynamical limit,[52] i.e., the infinite system, we have systematically underestimated.

### D. Surface energy

The surface energy, as previously defined, is now given by

$$\gamma(T)=\frac{1}{A(T)}\sum_{l=1}^{N_z'}\langle N_l\rangle_T(\langle\varepsilon_l\rangle_T-\langle\varepsilon_b\rangle_T), \tag{6}$$

where $\langle\varepsilon_l\rangle_T$ is the average interaction energy of an atom in layer $l$, $\langle\varepsilon_b\rangle_T$ is the average interaction energy of an atom in the bulk, $\langle N_l\rangle_T$ is the average number of atoms in layer $l$, and the summation is over all layers $N_z'$ for which $\langle\varepsilon_l\rangle_T\neq\langle\varepsilon_b\rangle_T$. $A(T)$ is the surface area of the computational cell at temperature $T$.

The calculated surface energies, Fig. 8, are roughly constant, at low temperatures, before increasing rapidly above 600 K. At low temperatures the surface energy is caused by the loss of neighbors for the surface atoms, with a contribution from surface relaxations. At higher temperatures there are additional contributions coming first from the increased anharmonicity (plus the harmonic enhancement) of the surface vibrations, and then from the presence of surface defects. Under these conditions several layers may contribute to the surface energy.

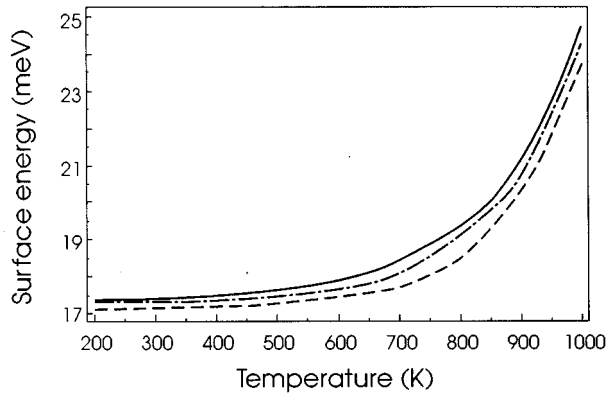


FIG. 8. Surface energy as a function of temperature for the (113) (solid line), (115) (dot-dashed line), and (117) (dashed line) surfaces. At low temperatures the surface energy is nearly constant (arising from the loss of neighbors for the surface atoms), but then increases rapidly above 600 K with the formation of surface defects with step meandering.

The surface energy is the sum over the excess energy per atom per layer, i.e., $\langle\varepsilon_l\rangle_T-\langle\varepsilon_b\rangle_T$, these are shown explicitly for the (115) surface in Fig. 9, for the adlayers and first six partial layers. Up to 600 K, the excess energies of all layers are approximately constant. Above 600 K, we see the appearance of adatoms with large excess free energies. However, below ~700 K, the concentration of such atoms is low, Fig. 5, and their contribution to the surface energy is expected to be small. The initial increase in surface energy is then due to the increasing excess energies of surface and subsurface layers due to increasing anharmonicity. At very high temperatures, close to the bulk melting point, the excess energies of the adlayers and surface layers decrease. This is caused by the increased coordination of these atoms with the formation

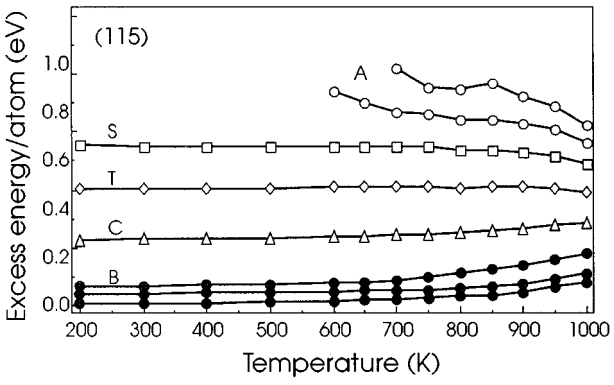


FIG. 9. The average excess energy per atom as a function of layer for the (115) surface. We now see the increased surface energy above 600 K is due to the presence of an increasing number of adatoms ($A$), see Fig. 5, with high excess energies. The decrease in the excess energies of the adatoms with temperature is due to the enhanced coordination arising from with the increased occupation of adlayers.

of a liquidlike layer. The large number of such adatoms though now make the dominant contribution to the surface energy. Notice also that the excess energy of the subsurface layers continues to increase.

### E. Structure factors

In order to study the translational order of the surface during the disordering processes, we have calculated the in-plane layer-dependent structure factor, defined as

$$S_l(\mathbf{k}) = \frac{1}{N_l} \sum_{i=1}^{N_l} \exp[i\mathbf{k}\cdot\mathbf{r}_i], \tag{7}$$

where $\mathbf{k}$ is a reciprocal lattice vector parallel to the surface, and the sum runs over all atoms, with position vectors $\mathbf{r}_i$ in layer $l$. Using $S_l(\mathbf{k})$, we can obtain an order parameter for the surface layers, $\langle|S_l(\mathbf{k})|^2\rangle$, where the averaging is over the MD trajectory. $\langle|S_l(\mathbf{k})|^2\rangle$ probes the local thermal disorder within a layer, being equal to one for an ordered layer at $T=0$, and near zero for a totally disordered or molten layer. It is, however, not sensitive to the nature of the disorder; lattice vibrations, vacancy formation, and melting all reduce it from unity. Notice that the existence of vacancies does not directly affect the order parameter, since it is normalized at each time step using the instantaneous layer occupation $N_l$. Vacancies do have an indirect effect by inducing distortions in the surface region and by allowing the remaining atoms in a layer to disorder.

In Fig. 10, the calculated order parameters in the $x$ and $y$ directions, perpendicular and parallel to the step edges, are presented as functions of temperature for the three stepped surfaces. For each surface the order parameters of the first $3(m+1)$ partial layer are shown. In the $y$ direction, parallel to the step edges, the reciprocal lattice vector is the same for all three surfaces. In the $x$ direction, perpendicular to the steps, the reciprocal lattice vector decreases in magnitude with increasing terrace width. Decreasing the size of the reciprocal lattice vector increases the length scale over which the order parameter is measured. As a result, the calculated structure factor in the $x$ direction for the (113) decreases more rapidly with temperature than for the (115) surface, which in turn appears more disordered than the (117) surface. Similarly, all three surfaces look more ordered in the $x$ direction, compared to the $y$ direction, because of the shorter reciprocal lattice vectors. This makes the $x$ order parameter relatively insensitive to disorder.

The behavior of the order parameter, in both the $x$ and $y$ directions, exhibits two distinct regimes. At low temperatures, $\langle|S_l(\mathbf{k})|^2\rangle$ shows a slow monotonic decrease with increasing temperature, for all layers. The deviation of the order parameter from unity originates from thermal vibrations and the decrease near the surface reflects the enhanced vibrational amplitudes of the surface atoms. In the harmonic approximation of solids (the Debye approximation),[53] $\ln\langle|S_l(\mathbf{k})|^2\rangle$ is proportional to $T$. Deviations from the linear dependence on temperature can be explained in terms of anharmonic vibrational effects, which introduce terms proportional to $T^2$ and $T^3$ into the expression for $\ln\langle|S_l(\mathbf{k})|^2\rangle$. At higher temperatures, the $\langle|S_l(\mathbf{k})|^2\rangle$ decrease more rapidly, both for the bulk due to enhanced vibrational amplitudes and in particular for the surface layers due to further enhanced vibrations, and the generation of defects and disorder. For the surface layers, the behavior of the order parameter cannot be fitted by the above mentioned expression for $\ln\langle|S_l(\mathbf{k})|^2\rangle$ because of the onset of defects and disorder.

Parallel to the step edges there is a clear grouping of the partial layers, and below the transition temperatures there is again evidence of pinning of the first and last partial layers forming the terraces on the (115) and (117) surfaces, which disappears once the surface layers start to completely disorder.

The exact nature of the disordering on these surfaces cannot be determined from the calculated order parameter; however, since there is already a considerable number of adatoms present on the respective surfaces at these temperatures, and the order parameter is normalized by the layer occupation, we can conclude that this disordering is not directly due to the roughening transition and the disordering of the step edges, but rather to the melting transition and the disordering of the surface, or at least that the surface melting is the dominant effect being observed. This is a reasonable interpretation since all $m+1$ surface layers on a $(11\{2m+1\})$ surface are seen to disorder at the same temperature. From the order parameter we estimate the surface disorder-melting temperatures for the (113), (115), and (117) surfaces to be $875\pm25$, $900\pm25$, and $925\pm25$ K, respectively.

Above the transition temperatures there is a gradual layer-by-layer disordering and/or melting of all the surfaces. This can be seen more clearly in Fig. 11, where $\langle|S_l(\mathbf{k})|^2\rangle$ is plotted as a function of layer for the (117) surface. As the temperature is increased, first the top $m+1$ partial layers start to melt, then the next $m+1$ partial layers melt, and so on into the bulk. At high temperatures, just below the bulk melting point, we are left with a completely disordered (molten) surface, separated from a still reasonably well ordered substrate by a partially melted full layer. The enhanced ordering of the deepest layers is due to the presence of the static substrate.

To see the actual roughening transition it is necessary to redefine slightly the above expression for $S_l(\mathbf{k})$, such that $\mathbf{k}$ is a reciprocal lattice vector perpendicular to the step edge and, by design, of equal length on all three surfaces, $\mathbf{r}_j$ is now the displacement of the step-edge atom (irrespective of layer) at position $j$ along the step, from the position of the step edge in the ordered phase (corrected for thermal relaxation and vibrations), and the sum is over all atoms forming the step edges. These new results are shown in Fig. 12. The loss of order on the surfaces is now seen at lower temperatures, firstly on the (117), then the (115), and lastly the (113), at $725\pm25$ K, and is the direct result of the surface roughening transition.

## V. STEP DYNAMICS

### A. Step-edge position

The histograms shown in Fig. 13 show the displacement of the step-edge atoms in terms of the number of atomic rows forwards and backwards from their positions in the ordered phase. As the temperature increases above 600 K, so does the number of kinks and the degree of step meandering that is reflected in the broadening of the distributions. At all

temperatures there is a symmetrical distribution of the step-edge position about the equilibrium terrace width, a displacement of zero, showing there to be no collapse of the step structure consistent with a repulsive interaction between steps. At high temperatures this repulsion is principally entropic in origin.

As the width of the terraces increases then so does the possibility of greater displacements of the step edge; this effect can also be seen in the calculated layer occupations, Fig. 5. In general, if the terraces are $m+1$ atomic rows wide, then the maximum forward displacement of the step edge at high temperatures is equal to $m$ atomic rows, while the maximum backward displacement is roughly $m+1$ atomic rows. These values should only be taken as an indication of the respective step-edge displacements. Even though the average terrace width of the surfaces, and therefore the maximum possible step-edge displacements, is structure dependent, the finite size of the computational cells and the periodic boundary conditions impose serious limitations on the extent of the step meandering in simulations of such systems.

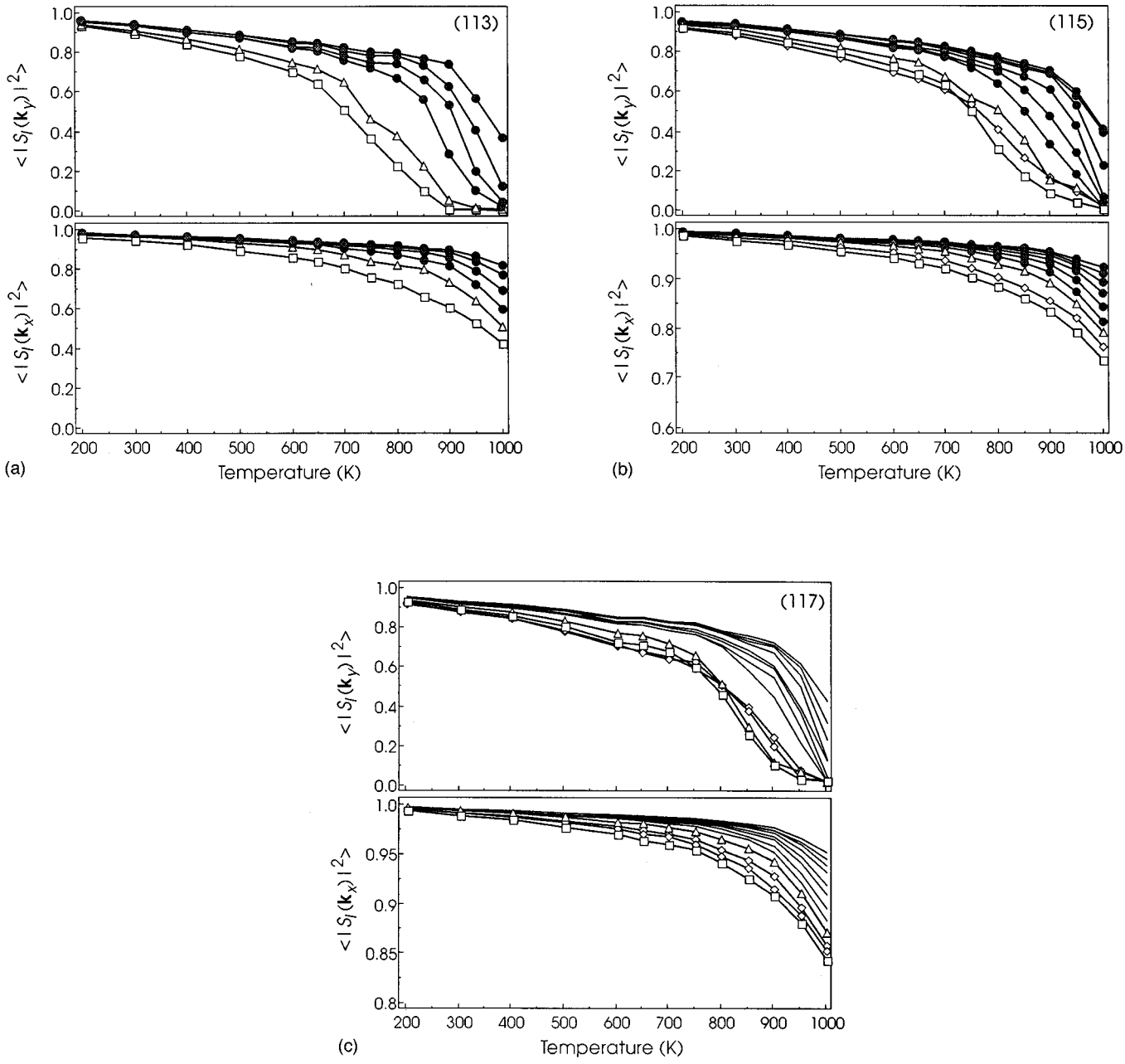


FIG. 10. Calculated order parameters parallel ($y$ direction) and perpendicular ($x$ direction) to the steps, for the first $3(m+1)$ crystal layers on the (a) (113), (b) (115), and (c) (117) surfaces. The recipical lattice vectors in the $y$ and $x$ directions are $2\pi/a$ and $2\pi/b$, respectively, where $a$ is the interatomic spacing atom the step and $b$ the step separation. That the surfaces appear more ordered in the $x$ direction with increasing terrace width is due to the decreasing magnitude of the reciprocal lattice vector. The simultaneous disordering of the $(m+1)$ crystal layers on the $(11\{2m+1\})$ surface with increasing temperature is distinct from the disordering of the step edges associated with the roughening transition. The total disordering of the surface is therefore attributed to the surfaces melting transition. The disorder-melting temperatures for the (113), (115), and (117) surfaces are estimated to be $875\pm25$, $900\pm25$, and $925\pm25$ K, respectively.

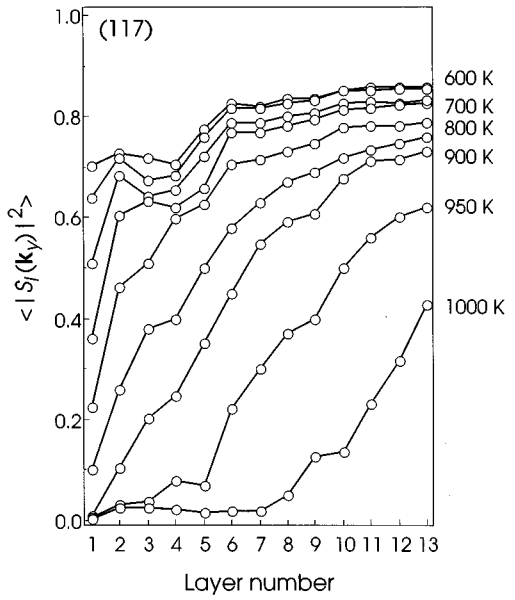


FIG. 11. Order parameter parallel ($y$ direction) to the steps as a function of layer for the (117) surface at several temperatures (in steps of 50 K). The surface is seen to disorder and/or melt in a layer-by-layer fashion, where a layer refers to $m+1$ crystal layers, starting from the surface.

### B. Step correlation functions

The spatial and time dependence of fluctuations in the step positions can be determined by calculating the step correlation functions $F(y)$ and $F(t)$, which are a measure of the average width of the steps.[2,5,15] For spatial fluctuations the step correlation function $F(y)$ is defined by

$$F(y)=\langle[R_x(y+y_0)-R_x(y_0)]^2\rangle, \tag{8}$$

where $R_x(y_0)$ is the displacement of the step edge atom at some coordinate $y_0$, and $R_x(y+y_0)$ is the displacement of the step-edge atom a distance $y$ along the same step. The average is over all pairs of atoms within the same step, all steps, and all configurations. Similarly for the step fluctuations in time the correlation function $F(t)$ is defined by

$$F(t)=\langle[R_x(y_0,t+t_0)-R_x(y_0,t_0)]^2\rangle, \tag{9}$$

where $R_x(y_0,t_0)$ is the displacement of the step edge at position $y_0$ at time $t_0$, and $R_x(y_0,t+t_0)$ is the displacement of the step edge at a later time $t+t_0$. The average is now over all positions $y_0$ and times $t_0$.

Both correlation functions can be measured using an STM.[15–21] The conventional method of imaging the surface is to scan the tip across a region of the surface. Since the STM does not provide an instantaneous image of the surface, consecutive scan lines under such conditions represent spatial fluctuations of the steps as well as movement in time. Because the step motion is fast relative to the scan speed, the tip finds the step edge in a different position in each scan line, giving rise to a ''frizzy'' appearance of the steps.[17,18,20] An alternative method of imaging the surface, which separates the influence of the spatial fluctuations from the fluctuations in time, is to repeatedly scan the tip over the same line perpendicular to the step edges, giving a time sequence of the step-edge positions. Giessen-Seibert *et al.*[20] recently showed the equivalence of the two step correlation functions [$F(y)$ calculated from conventional images and $F(t)$ from time images] for step fluctuations on Cu(1 1 19) surfaces at $T>T_R$. Thus the fluctuations in the step positions in conventional tunneling images are entirely due to the time dependence.

For a surface with isolated or widely spaced steps (which would have a very low roughening temperature), $F(y)$ is a linear function of $y$, and describes the random walk of free (unhindered) steps. If, however, $F(y)$ is comparable to the square of the average step separation, the noncrossing constraint of neighboring steps prevents each step from making a random walk and $F(y)$ then diverges logarithmically.

The exact time dependence for motion of the steps by different mechanisms (different rate limiting processes) have been modeled using Langevin dynamics.[22,23] If mass transport occurs solely along the steps, then the resulting motion of a step will be strongly correlated between different positions along the step. The fluctuations in a step will be slow, and the correlation function $F(t)$ is proportional to $t^{1/4}$. If, however, the steps diffuse by exchange with a reservoir of atoms on the neighboring terraces, then the correlations in the step fluctuations are expected to be weak and the motion of the steps will be correspondingly faster. In this case the correlation function $F(t)$ is proportional to $t^{1/2}$.

The calculated step correlation function $F(y)$ for the three surfaces at several temperatures[54] is shown in Fig. 14. The step meandering process is inhibited to a large degree by the periodic boundary conditions, and the maximum $y$ value is

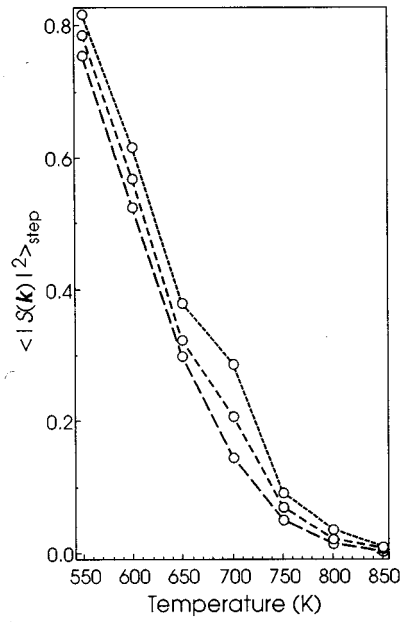


FIG. 12. Calculated order parameter for the step edge atoms on the (113) (dotted line), (115) (short-dashed line), and (117) (long-dashed line) surfaces as a function of temperature. From the construction of the structure factor, as described in the text, the observed disordering is now the result of the roughening transition. The roughening temperature is seen to decrease with increasing terrace width, and is of the order of 725±25 K for the three surfaces.

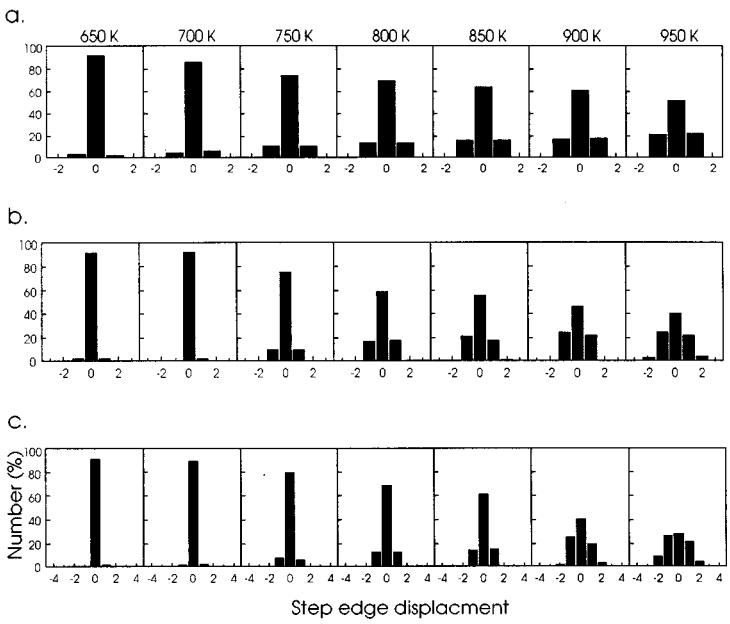


FIG. 13. Histograms of the step edge displacement for the (a) (113), (b) (115), and (c) (117) surfaces. The broadening of the distribution with increasing temperature is due to increased step meandering. At low temperatures the step meandering is limited by the energetic repulsion between the steps; at high temperatures it is limited by the entropic repulsion between the steps. The distribution is symmetric at all temperatures, and there is no collapse of the step structure, even at the very highest temperatures.

fixed equal to half the size of the computational box in the direction parallel to the steps. In principle, the step roughening temperature $T_R$ can be determined from the logarithmic divergence of $F(y)$ for large $y$. At the roughening temperature the step correlation function has the form[5]

$$F(y)=A(T)\ln(y)+B, \tag{10}$$

where $A(T_R)=2/\pi^2$ is a universal constant [if $T>T_R$ then $A(T)>2/\pi^2$], and $B$ is a nonuniversal constant. From fitting the data to the above relationship we estimate the roughening temperature to be between 900 and 950 K for the (113) surface, 850 and 900 K for the (115) surface, and 800 and 850 K for the (117) surface. These values are considerably higher than other estimates based on the concentrations of adatoms, and the structure factors for the step edges. Experimentally the logarithmic divergence of $F(y)$ is measured over macroscopic distances (of the order of hundreds of angstrom) and the small surface area of the systems studied thus precludes an accurate determination of this behavior, and hence of the roughening temperature. As a consequence, these results (and all MD simulations of finite systems) can only provide a qualitative guide (an upper limit) to the roughening temperature although we believe the trends from surface to surface to be real.

The calculated step correlation functions for fluctuations in time for the three surfaces[54] all show a time dependence proportional to $t^n$, Fig. 15. However, we find that the power $n$ is dependent on the both the surface and the temperature, Table IV. Since $n$ is greater than 0.25 for the three surfaces at all temperatures, we conclude that surface diffusion is intrinsically two dimensional, and that step fluctuations occur by exchange with a reservoir of atoms, in this case provided by the adjacent steps. This is verified by analysis of snapshots of the atomic configurations from the simulations, and the calculated layer diffusion coefficients.

The $t^{1/2}$ power law for step fluctuations is derived assuming widely spaced, noninteracting, steps.[22] The inclusion of step-step interactions will limit the amount of step meandering leading to an increase in the characteristic time scale for step fluctuations, reducing $n$. At any finite temperature, the larger the interactions, i.e., the closer the steps, the larger the effect. As the temperature is increased, the energetic step-step interactions will be gradually overwhelmed by the thermal energy of the atoms, causing the time dependence of the fluctuations to increase ultimately to $n\rightarrow\frac{1}{2}$.

However, at higher temperatures above 750 K for the (113) surface and 800 K for the (115) and (117) surfaces, the calculated values of $n$ again decrease. This effect is due to entropic repulsion (the topological constraint that the meandering steps cannot cross); the $t^{1/2}$ law is therefore only strictly valid when $F(t)$ is small compared to the square of the mean terrace width. (The extent of step meandering with increasing temperature can be seen in Figs. 5, 13, and 14.) Thus as the temperature increases beyond the roughening transition the extent of the step meandering increases resulting in a gradual disordering of the terraces as a prelude to surface melting. As one would expect, the temperature ordering for this effect, first the (113), then (115), and finally the (117) surface, then reflects that of the surface melting transition.

### C. Diffusion

To compare the dynamical properties of the three surfaces during the roughening and melting transitions we have studied the layer diffusion coefficients in the directions perpendicular and parallel to the steps in the plane of the surface, and in the direction normal to the surface plane. The layer diffusion coefficient is defined by the long-time behavior of the mean-square displacement of the atoms calculated from the atomic trajectories:

$$D_{\alpha,l}=\lim_{t\rightarrow\infty}\frac{R^2_{\alpha,l}(t)}{2dt}, \tag{11}$$

where $d=1$ is the dimensionality, $\alpha=x$ (i.e., $\perp$), $y$ (i.e., $\parallel$), and $z$, and $R^2_{\alpha,l}(t)$ is the MSD of an atom in layer $l$:

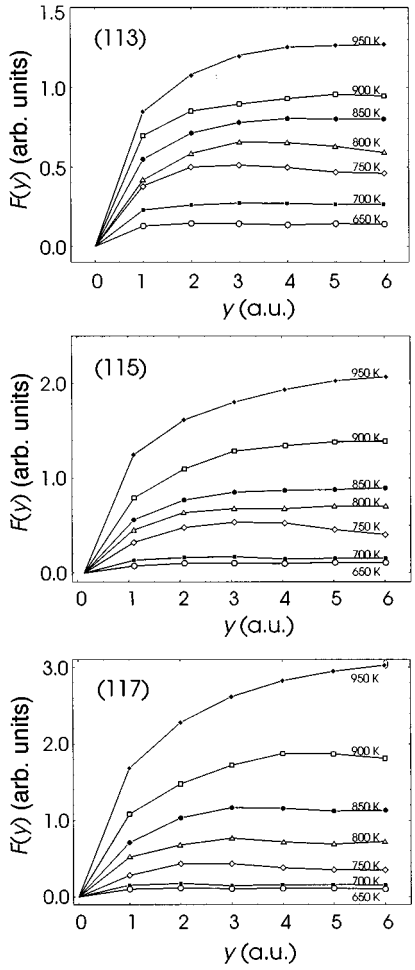


FIG. 14. Mean-square displacements of step position $F(y)$ as a function of position $y$ along the step for the (113), (115), and (117) surfaces. The maximum $y$ value is equal to half the size of the computational box in the direction parallel ($y$ direction) to the steps. The true logarithmic divergence of $F(y)$ for large $y$, which is observed only above 900, 850, and 800 K, for the (113), (115), and (117) surfaces, respectively, is then constrained by the finite size of the computational cells.

$$R_l^{(2)}(t)=\left\langle \frac{1}{n_l}\sum_{i\in l}\left[R_i(t+\tau)-R_i(\tau)\right]^2\right\rangle. \qquad (12)$$

The sum includes all atoms in layer $l$ at time $\tau$, and the average is over time origins $\tau$.

The layer diffusion coefficients are plotted in Fig. 16 for the adlayers and top $3\times(m+1)$ partial layers of each surface. Several features are apparent between 600 and 1000 K on all three surfaces. With the onset of step meandering, we see the formation of a mobile adlayer. The large layer diffusion coefficients in the direction parallel to the steps, $D_{\|}$, reflects the adatoms moving relatively quickly along the step edges (atomic hopping). This increased mobility is, however, not restricted to the direction parallel to the steps; $D_{\perp}$ also rises as atoms move backwards and forwards due to the step meandering. (There is also a marked increase in $D_z$, but this effect is much smaller than for either $D_{\|}$ or $D_{\perp}$.) This increased mobility between 600 and 800 K is largest on the (117) surface (not shown), which is generally the first to

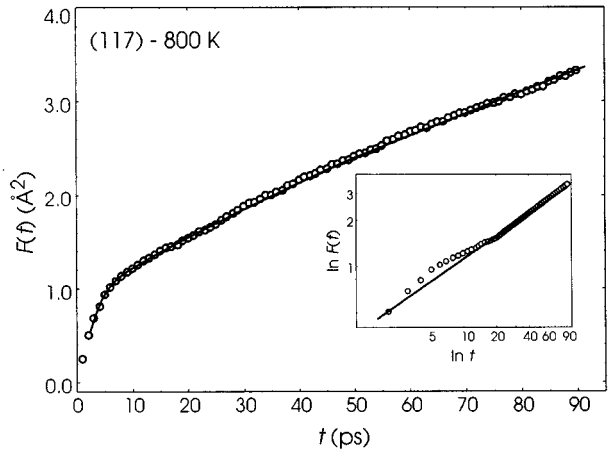


FIG. 15. Mean-square displacement of step position $F(t)$ as a function of time $t$ for the (117) surface at 800 K. The inset shows the same data on a logarithmic plot. The solid lines are power-law fits, $F(t)\propto t^n$, where $n=0.49\pm0.03$, see Table IV. Notice that $F(t)$ starts linearly and crosses over to $t^{1/2}$.

show signs of step roughening due to the weaker step-step repulsion present. On all three surfaces, the layers of atoms, which in the ordered phase form the step edges (and the terraces), also show increased mobility, and for these layers $D_{\|}\approx D_{\perp}$. The increased mobility parallel to the steps is due to the presence of vacancies in these rows, whereas the increased mobility perpendicular to the steps reflects the movement (exchange) of atoms between the steps (and terraces).

As the temperature increases then so does the extent of the step meandering with the increased occupation of higher adlayers and the formation of deeper vacancies, Figs. 5 and 13. The increased occupation of an adlayer, and the subsequent occupation of the next adlayer, starts to limit the diffusion of atoms in that layer resulting in a decrease in layer diffusion coefficient parallel to the steps as that of the next adlayer increases. These higher adlayers also show increased mobility perpendicular to the steps, and in the $z$ direction.

These results are consistent with the two-dimensional diffusion of the atoms during the step meandering, as discussed previously. Although different diffusion mechanisms must prevail in the two directions, parallel and perpendicular to the steps, these mechanisms must be similar on all three surfaces since there is no great difference between the respective results.

At temperatures above 950 K, $D_{\|}\approx D_{\perp}\approx 2D_z$ for all exposed surface layers; that is atoms can now move as freely perpendicular to the steps as parallel to them, and there is also a large degree of intermixing between the surface layers. This enhancement of the diffusion coefficients of the topmost surface layers relative to the deeper bulk layers at temperatures slightly below the bulk melting temperature is consistent with the idea of surface melting, and the growth of a highly mobile liquidlike film on the surface. This is more apparent in Fig. 17, where the diffusion coefficients are plotted as a function of depth at 1000 K. The equivalence of the diffusion coefficients in the $x$ and $y$ directions at this temperature implies a complete disintegration of step structure at the surface. Diffusion perpendicular to the surface is still, however, smaller than the in-plane diffusion, since the liq-

TABLE IV. The calculated exponents $n$ for the time dependence $t^n$ of the step fluctuations. Values have an associated error of $\pm 0.03$.

| | Exponent in the time correlation function | | | | | |
|---|---|---|---|---|---|---|
| Surface | 650 K | 700 K | 750 K | 800 K | 850 K | 900 K |
| (113) | 0.31 | 0.38 | 0.39 | 0.35 | 0.33 | 0.29 |
| (115) | 0.34 | 0.37 | 0.43 | 0.46 | 0.41 | 0.36 |
| (117) | 0.34 | 0.38 | 0.45 | 0.49 | 0.44 | 0.37 |

uidlike layer is only a few atomic layers thick, approximately 2 and 3 full layers, i.e., ~5 Å, on all three surfaces.

### D. Diffusion mechanisms

Firstly, parallel to the step edges, the adatoms move by atomic hopping. No adatoms were observed to hop away from the step edges on to the terraces; to do so would involve a reduction in coordination, and hence a large initial activation energy barrier, which would be further increased by the step-step repulsion. The only atomic hopping events observed perpendicular to the steps were predominantly on the (115) and (117) surfaces, and involved an atom moving forward one atomic row out of the step edge creating a vacancy. These step edge vacancies then diffuse by a neighboring atom hopping into the site. Again vacancies were never observed to diffuse away from the step edges. However, any vacancies in the terraces are quickly absorbed into the step edges. A few exchange events parallel to the steps were also observed in which the adatom on the step edge displaces a corner atom from the underlying terrace. Unlike for self-diffusion on the (100) surface of aluminum,[39] the coordination of the exchanging atoms on the vicinal surfaces remains high due to the presence of the neighboring step-edge atoms, effectively stabilizing the exchange process. Perpendicular to the step edges, diffusion occurs by elaborate exchange

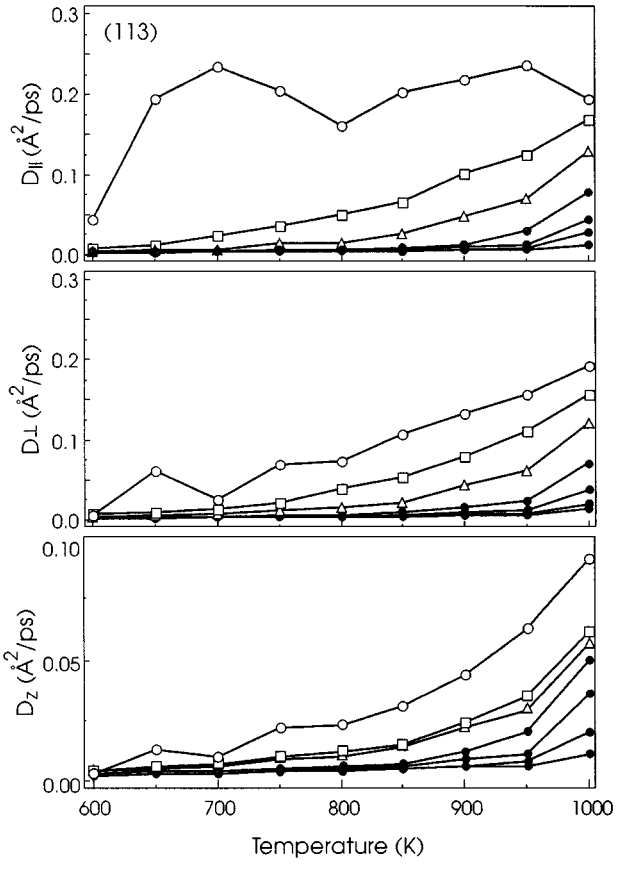


FIG. 16. Calculated layer diffusion coefficients, as a function of temperature, in the $y$ (i.e., $\parallel$), $x$ (i.e., $\perp$), and $z$ directions for the $2m$ adlayers and $3(m+1)$ crystal layers on the (113) surface. The symbols are defined in Fig. 5. The adlayers are highly mobile parallel, and also perpendicular, to the step edges. For the $(m+1)$ surface layers at all temperatures, and the adlayers close to the surface melting temperature, $D_{\parallel} \approx D_{\perp} \approx 2D_z$. Thus diffusion during step meandering is generally two dimensional.

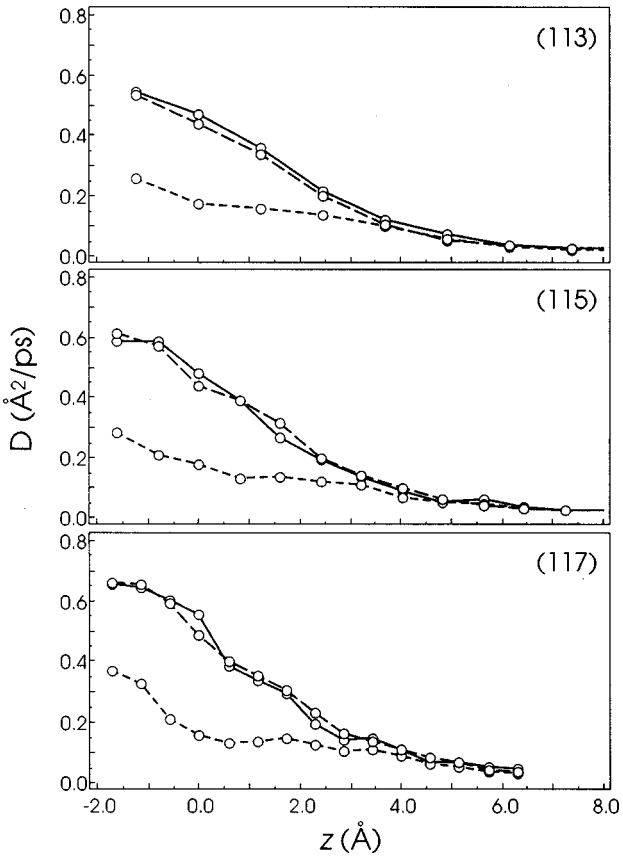


FIG. 17. Layer diffusion coefficients, $D_y$ (solid line), $D_x$ (long-dashed line), and $D_z$ (short-dashed line) as a function of position $z$ at 1000 K for the (113), (115), and (117) surfaces. The large diffusion coefficients of the adlayers and surface layers reflect the formation of a highly mobile liquidlike layer at the surface. The thickness of this layer, ~5 Å, is the same on all three surfaces.

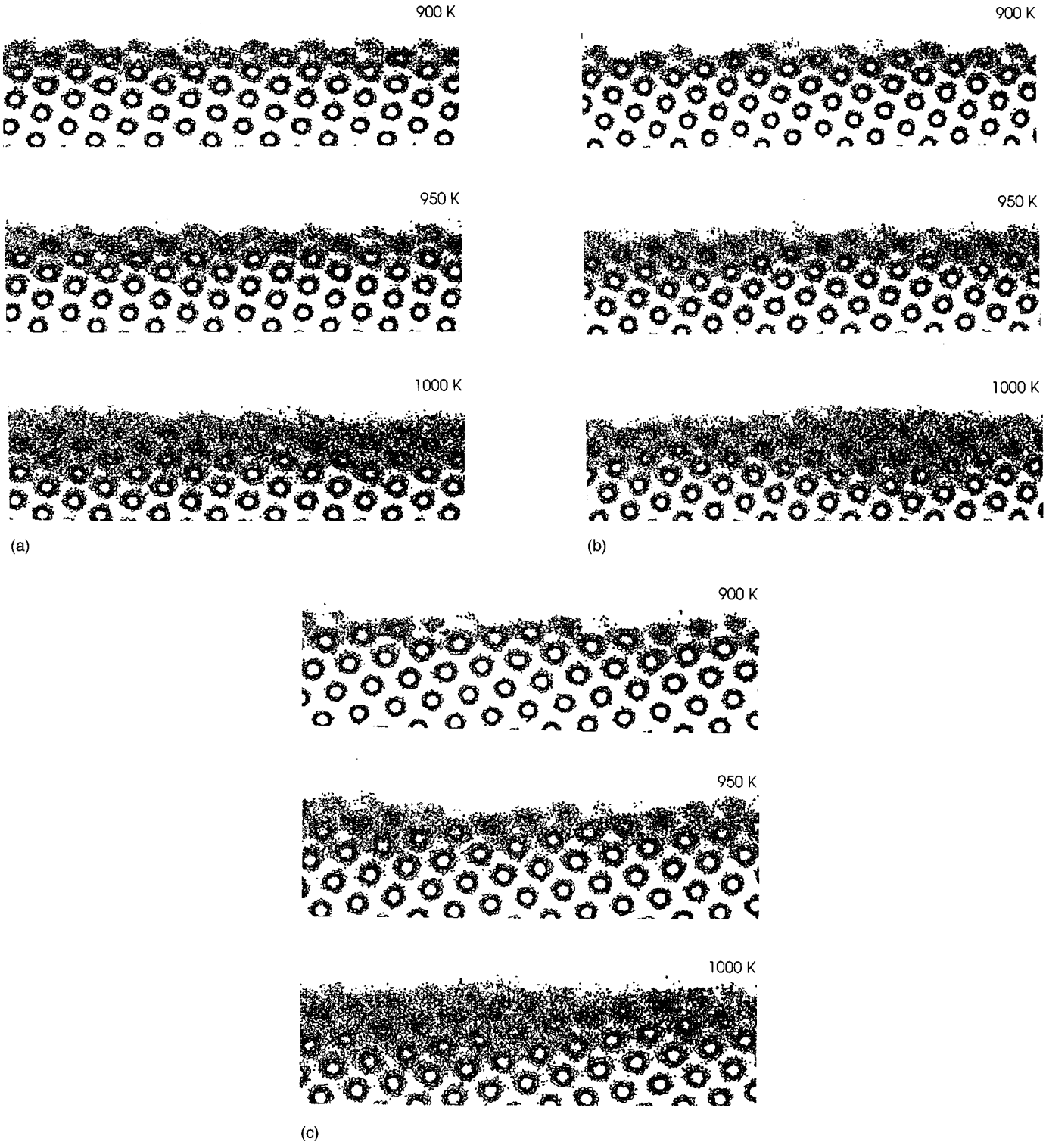


FIG. 18. Contour plots of the average atomic density projected onto the $x$-$z$ plane for the (a) (113), (b) (115), and (c) (117) surfaces. The highest densities have not been shown and as a result, the central parts of the atoms appear empty. The disappearance of the step structure and the formation of a diffuse liquidlike layer can be seen on all three surfaces above 900 K. Some oscillations in the thickness of this layer can be seen on the (113) surface at 950 K due to the corrugation of the underlying periodic potential.

mechanisms, involving chains of several atoms.[55] By this method atoms are able to move ''up'' and ''down'' the steps, frequently over more than one step at a time, especially on the (113) surface, which has the narrowest terraces. Chain slippages were also found to be a common way of creating new kinks in the step edges: A chain of atoms on a terrace would either move backwards one atomic row, leaving a vacancy in the step edge, while the first atom in the chain becomes an adatom on the higher terrace, or forwards one atomic row forming a new adatom at the step edge; the re-

sulting vacancy left by the end of the chain is quickly filled by a step-edge atom on the higher terrace falling down a level. The first of these two mechanisms was found to be the most frequent method of defect creation on the (113) surface.

### E. Solid-liquid interface

The presence of a liquidlike layer on the surfaces, at temperatures approaching the bulk melting point, can be seen more clearly in the contour plots of the atomic density projected onto the $x$-$z$ plane, perpendicular to the steps, Fig. 18. As the temperature approaches the bulk melting point, the steps disappear (but do not collapse) with the formation of a broad diffuse layer at the surface. As we have already seen, from the calculated structure factors and diffusion coefficients for the layers, the surface melting occurs in a layer-by-layer fashion. The order for the surface melting follows that of the terrace width; the step structure disappears first on the (113) surface, then on the (115) surface, and finally on the (117) surface at temperatures between 900 and 1000 K. For all surfaces, at 1000 K, the liquidlike layer is broad but not uniform, suggesting weak faceting. Notice that even at 1000 K the atoms moving in the liquid layer close to the solid-liquid interface exhibit some residual crystal order due to the underlying periodic potential. The corrugation of the potential decreases with step density, but this does not appear to affect the thickness of the liquidlike layer at 1000 K on the three surfaces, although it is visible on the (113) surface at 950 K, and may be responsible for the observed oscillations in the thickness of the liquid layer.

## VI. DISCUSSION

The dynamics of the (113), (115), and (117) stepped surfaces of aluminum have been studied using the MD method with a realistic many-body potential that at 0 K gives reasonable predictions for the stability of the surfaces and the interactions between the steps. The principal result of this work is that these surfaces show two distinct forms of thermal disordering. Firstly, around 700 K the surfaces undergo a roughening transition, characterized by a disordering of the step-edge structure; the roughening temperature for the surfaces decreases with decreasing step density (decreasing step-step repulsion), i.e., $T_R^{(113)} > T_R^{(115)} > T_R^{(117)}$. Secondly, around 900 K the surfaces undergo a melting transition, characterized by a complete disordering of the surface; the melting temperature for the surfaces increases with decreasing step density (following the order of the surface stability), i.e., $T_M^{(113)} < T_M^{(115)} < T_M^{(117)} (< T_M^{(001)})$.

The stepped surfaces exhibit strongly anharmonic behavior. The anharmonicity manifests itself as an enhanced thermal expansion coefficient of the surface, and an anomalous increase in the vibrational amplitudes of the surface atoms. Above 600 K we also observe the formation of adatoms and vacancies associated with motion of the steps, and the onset of surface roughening. As the temperature is increased further, the amount of step meandering increases with the appearance of atoms in higher adlayers, and vacancies in deeper surface layers. There is then also a rapid increase in the surface energy above 600 K due to both the step meandering and the increased surface anharmonicity.

Identification of the rough phase in MD simulations is difficult because the small sample sizes and simulation times preclude the accurate determination of the logarithmic behavior of the step correlation function. Based upon the calculated structure factors for the step edges, the roughening temperatures for the (113), (115), and (117) surfaces of aluminum are estimated to be in the range $725 \pm 25$ K, with the ordering as above. These are lower than the values suggested by the spatial dependence of the fluctuations in the step-edge position, which should only be taken as upper limits on the true values.

The time dependences of the step fluctuations show a power-law behavior, $t^n$, where $0.25 < n \leqslant 0.5$, and diffusion on all three surfaces is essentially two dimensional. The atomic trajectories indeed show atoms moving parallel to the steps by atomic hopping and exchange, and perpendicular to the steps by the concerted motion of chains of atoms that can extend over more than one terrace. However, at temperatures close to $T_R$ the energetic repulsion between the steps reduces the time dependence of the step fluctuations, reflecting a decrease in the amount of step meandering compared to that of a system of noninteracting steps.

From studies of the low-index surfaces of metals, it is generally believed that anharmonic effects control the dynamics of the surface roughening and melting transitions: The large vibrational amplitudes of the surface atoms result in the initial disordering of a surface with the creation of adatoms and vacancies; these vacancies then allow the remaining surface atoms to disorder, leading eventually to surface melting. Note, however, that the anharmonicity alone does not make the surfaces vibrationally unstable. The vibrations of the surface atoms must also be coupled to an ''escape route'' from the ordered surface structure. Such a path exists on the open (110) surface, which shows signs of roughening, but not on the closely packed (100) surface, which does not, although both show comparable surface anharmonicity.[42] On stepped surfaces, the appearance of adatoms and vacancies is again correlated with the increasing vibrational amplitudes of the surface atoms, most importantly in the direction perpendicular to the step edges, consistent with the above picture.

The first signs of surface roughening are restricted to the step edges, the terraces remaining well ordered. As the temperature increases and the thermal energy of the atoms overcomes the repulsion between steps then the extent of the step meandering increases, leading to a broader distribution of the step-edge position and the disordering of more and more of the atomic rows forming the terraces. The dynamics of the step motion is now governed by the entropic repulsion between steps, and the topological constraint that the meandering steps cannot cross. When the width of the step-edge distribution becomes greater than that of the terraces, then all the atoms in the surface are effectively disordered. Further increases in the temperature result in the disordering of more and more layers, i.e., layer-by-layer melting, and the formation of a broad diffuse interface at the surface. The estimated melting temperatures for (113), (115), and (117) surfaces of aluminum are $900 \pm 25$, $925 \pm 25$, and $950 \pm 25$ K, respectively. These are slightly larger than the values quoted earlier from the structure factors, which we interpret as the initial structural disordering of the topmost surface layers, preempting the surface melting.

**ACKNOWLEDGMENTS**

We would like to thank George Darling and Claudio Verdozzi for many interesting discussions and suggestions, and the Department of Computer Science, University of Liverpool, for the use of their computers on which these calculations were performed.

*Present address: Facultés Universitaires Notre-Dame de la Paix, Département de Physique, Rue de Bruxelles 61, B-5000 Namur, Belgium.

†Author to whom correspondence should be addressed. Fax: +44 151 708 0662. Electronic address: stephen@ssci.liv.ac.uk

[1] J. M. Kosterlitz and D. J. Thouless, J. Phys. C **6**, 1181 (1973); J. M. Kosterlitz, *ibid.* **7**, 1046 (1974).

[2] J. D. Weeks, in *Ordering in Strongly Fluctuating Condensed Matter Systems*, edited by T. Riste (Plenum, New York, 1980); H. van Beijever and I. Nolder, in *The Structure and Dynamics of Surfaces*, edited by W. Schommers and P. van Blanckenhager (Springer, Berlin, 1987), Vol. II; K. Kern, in *The Chemical Physics of Solid Surfaces*, edited by D. A. King and D. P. Woodruff (Elsevier, Amsterdam, 1994), Vol. 7; J. Lapujoulade, Surf. Sci. Rep. **20**, 191 (1994).

[3] J. Lapujoulade, J. Perreau, and A. Kara, Surf. Sci. **129**, 59 (1983).

[4] J. Villain, D. R. Grempel, and J. Lapujoulade, J. Phys. F **15**, 809 (1985).

[5] D. Gorse and J. Lapujoulade, Surf. Sci. **162**, 847 (1985).

[6] E. H. Conrad, R. M. Aten, D. S. Kaufman, L. R. Allen, T. Engel, M. den Nijs, and E. K. Reidel, J. Chem. Phys. **84**, 1015 (1986); **85**, 4756 (1986).

[7] F. Fabre, D. Gorse, J. Lapujoulade, and B. Salanon, Europhys. Lett. **3**, 737 (1987).

[8] F. Fabre, D. Gorse, B. Salanon, and J. Lapujoulade, J. Phys. (Paris) **48**, 1017 (1987).

[9] B. Salanon, F. Fabre, J. Lapujoulade, and W. Selke, Phys. Rev. B **38**, 7385 (1988).

[10] F. Fabre, B. Salanon, and J. Lapujoulade, Solid State Commun. **64**, 1125 (1987).

[11] E. H. Conrad, L. R. Allen, D. L. Blanchard, and T. Engel, Surf. Sci. **187**, 265 (1987).

[12] D. L. Blanchard, D. F. Thomas, H. Xu, and T. Engel, Surf. Sci. **222**, 477 (1989).

[13] K. S. Liang, E.-B. Sirota, K. L. D'Amico, G. J. Hughess, and S. K. Sinha, Phys. Rev. Lett. **59**, 2447 (1987).

[14] I. K. Robinson, E. H. Conrad, and D. S. Reed, J. Phys. (Paris) **51**, 103 (1990).

[15] B. S. Swartzentruber, Y.-W. Mo, R. Kariotis, M. G. Lagally, and M. B. Webb, Phys. Rev. Lett. **65**, 1913 (1990).

[16] X. S. Wang, J. L. Goldberg, N. C. Bartelt, T. L. Einstein, and E. D. Williams, Phys. Rev. Lett. **65**, 2430 (1990).

[17] J. Frohn, M. Giesen, M. Poensgen, J. F. Wolf, and H. Ibach, Phys. Rev. Lett. **67**, 3543 (1991).

[18] M. Poensgen, J. F. Wolf, J. Frohn, M. Giesen, and H. Ibach, Surf. Sci. **274**, 430 (1992).

[19] L. Kuipers, M. S. Hoogeman, and J. W. M. Frenken, Phys. Rev. Lett. **71**, 3517 (1993).

[20] M. Giesen-Seibert, R. Jentjens, M. Poensgen, and H. Ibach, Phys. Rev. Lett. **71**, 3521 (1993).

[21] J. C. Girard, S. Gauthier, S. Rousset, W. Sacks, S. de Cheveigné, and J. Klein, Surf. Sci. **301**, 245 (1994).

[22] N. C. Bartelt, T. L. Einstein, and E. D. Williams, Surf. Sci. Lett. **240**, L591 (1990); N. C. Bartelt, J. L. Goldberg, T. L. Einstein, and E. D. Williams, Surf. Sci. **273**, 252 (1992).

[23] A. Pimpinelli, J. Villain, D. E. Wolf, J. J. Métois, J. C. Heyraud, I. Elkinani, and G. Uimin, Surf. Sci. **295**, 143 (1993).

[24] E. D. Williams, Surf. Sci. **299/300**, 502 (1994).

[25] C. Jayaprakash, C. Rottman, and W. F. Saam Phys. Rev. B **39**, 6549 (1984).

[26] J. M. Blakely and R. L. Schwoebel, Surf. Sci. **26**, 321 (1971).

[27] V. I. Marchenko and A. Ya Parshin, Pis'ma Zh. Eksp. Teor. Fiz. **31**, 767 (1980) [JETP Lett. **31**, 724 (1981)].

[28] A. C. Refeild and A. Zangwill, Phys. Rev. B **46**, 4289 (1992).

[29] R. Stumpf and M. Scheffler, Phys. Rev. Lett. **72**, 254 (1994).

[30] E. D. Williams and N. C. Bartelt, Science **251**, 393 (1991).

[31] B. Loisel, D. Gorse, V. Pontikis, and J. Lapujoulade, Surf. Sci. **221**, 365 (1989).

[32] D. Wolf, Surf. Sci. **226**, 389 (1990); D. Wolf and J. A. Jaszczak, *ibid.* **277**, 301 (1992).

[33] Z.-J. Tian and T. S. Rahman, Phys. Rev. B **47**, 9751 (1993).

[34] C.-L. Liu and J. B. Adams, Surf. Sci. **294**, 211 (1993).

[35] R. C. Nelson, T. L. Einstein, S. V. Khare, and P. J. Rous, Surf. Sci. **295**, 462 (1993).

[36] K. D. Hammond and R. M. Lynden-Bell, Surf. Sci. **278**, 437 (1992).

[37] G. Bilalbegovic, F. Ercolessi, and E. Tosatti, Surf. Sci. **280**, 335 (1993).

[38] K. W. Jacobsen, J. K. Nørskov, and M. J. Puska, Phys. Rev. B **35**, 7423 (1987); K. W. Jacobsen, Comments Condens. Matter Phys. **14**, 129 (1988).

[39] P. J. Feibelman, Phys. Rev. Lett. **65**, 729 (1990); P. A. Gravil and S. Holloway, Surf. Sci. **294**, 211 (1993).

[40] P. Stoltze, J. K. Nørskov, and U. Landman, Phys. Rev. Lett. **61**, 440 (1988); Surf. Sci. **22**, L693 (1989); P. Stoltze, J. Chem. Phys. **92**, 6306 (1990).

[41] A. W. Denier van der Gon, D. Frenkel, J. W. M. Frenken, R. J. Smith, and P. Stoltze, Surf. Sci. **256**, 385 (1991).

[42] A. M. Molenbroek and J. W. M. Frenken, Phys. Rev. B **50**, 11 132 (1994).

[43] H. Häkkinen and M. Manninen, Phys. Rev. B **46**, 1725 (1992).

[44] See, for example, M. P. Allen and D. J. Tildesley, *Computer Simulations of Liquids* (Oxford University Press, Oxford 1987).

[45] H. L. Davis and J. R. Noonan, Surf. Sci. **126**, 245 (1983).

[46] P. R. Watson and K. A. R. Mitchell, Surf. Sci. **203**, 323 (1988).

[47] D. Gorse, J. Lapujoulade, and V. Pontikis, Surf. Sci. **178**, 343 (1986).

[48] P. Zeppenfeld, K. Kern, R. David, and G. Comsa, Phys. Rev. Lett. **62**, 63 (1989).

[49] Y. Cao and E. H. Conrad, Phys. Rev. Lett. **64**, 447 (1990).

[50] E. T. Chen, R. N. Barnett, and U. Landman, Phys. Rev. B **41**, 439 (1990).

[51] R. N. Barnett and U. Landman, Phys. Rev. B **44**, 3226 (1991).

[52] M. O. Robbins, G. S. Grest, and K. Kremer, Phys. Rev. B **42**, 5579 (1990).

[53] J. M. Ziman, *The Principles of the Theory of Solids* (Cambridge University Press, Cambridge, 1965).

[54] P. A. Gravil and S. Holloway, Surf. Rev. Lett. **11**, 611 (1994).

[55] P. A. Gravil, Ph.D. thesis, University of Liverpool, 1994.